



# In vitro grafting of hepatic spheroids and organoids on a microfluidic vascular bed

Flavio Bonanini<sup>1</sup> · Dorota Kurek<sup>1</sup> · Sara Previdi<sup>1</sup> · Arnaud Nicolas<sup>1</sup> · Delilah Hendriks<sup>2</sup> · Sander de Ruiter<sup>1</sup> · Marine Meyer<sup>1</sup> · Maria Clapés Cabrer<sup>1</sup> · Roelof Dinkelberg<sup>1</sup> · Silvia Bonilla García<sup>1</sup> · Bart Kramer<sup>1</sup> · Thomas Olivier<sup>1</sup> · Huili Hu<sup>2</sup> · Carmen López-Iglesias<sup>3</sup> · Frederik Schavemaker<sup>1</sup> · Erik Walinga<sup>1</sup> · Devanjali Dutta<sup>2</sup> · Karla Queiroz<sup>1</sup> · Karel Domansky<sup>1</sup> · Bob Ronden<sup>1</sup> · Jos Joore<sup>1</sup> · Henriette L. Lanz<sup>1</sup> · Peter J. Peters<sup>3</sup> · Sebastiaan J. Trietsch<sup>1</sup> · Hans Clevers<sup>2</sup> · Paul Vulto<sup>1</sup>

Received: 16 November 2021 / Accepted: 14 May 2022 / Published online: 15 June 2022  
© The Author(s) 2022

## Abstract

With recent progress in modeling liver organogenesis and regeneration, the lack of vasculature is becoming the bottleneck in progressing our ability to model human hepatic tissues *in vitro*. Here, we introduce a platform for routine grafting of liver and other tissues on an *in vitro* grown microvascular bed. The platform consists of 64 microfluidic chips patterned underneath a 384-well microtiter plate. Each chip allows the formation of a microvascular bed between two main lateral vessels by inducing angiogenesis. Chips consist of an open-top microfluidic chamber, which enables addition of a target tissue by manual or robotic pipetting. Upon grafting a liver microtissue, the microvascular bed undergoes anastomosis, resulting in a stable, perfusable vascular network. Interactions with vasculature were found in spheroids and organoids upon 7 days of co-culture with space of Disse-like architecture in between hepatocytes and endothelium. Venous-occlusive disease was induced by azathioprine exposure, leading to impeded perfusion of the vascularized spheroid. The platform holds the potential to replace animals with an *in vitro* alternative for routine grafting of spheroids, organoids, or (patient-derived) explants.

**Keywords** In vitro grafting · Vascularization · Liver organoids and spheroids · Microfluidics

## Introduction

In the past few years, the ability to recapitulate features of human liver architecture and functionality *in vitro* has dramatically improved due to the use of three-dimensional culture methods. Spheroids and organoids are emerging as promising tools to study human organ development and regeneration, and can provide a model with enhanced

translatability for drug response studies [1, 2]. One of the key limitations of current *in vitro* liver models is the lack of structured and functional sinusoidal vascular networks to ensure proper oxygenation and nutrition [3]. In fact, the liver is a highly vascularized organ, where specialized liver sinusoidal endothelial cells (LSECs) represent one of the predominant cell types, comprising about 70% of the non-parenchymal cell population [4, 5]. Studies have shown that all avascular organoids and spheroids with a size of 100  $\mu\text{m}$  or larger are characterized by poor cell viability and functionality, which might translate into unstable and immature cultures [6, 7]. In addition, endothelial cells release angiocrine factors contributing to tissue growth, maturation, and functionality, as becomes apparent during organogenesis [8–10] and homeostasis [11, 12].

Various strategies have been pursued to introduce endothelial cells into liver microtissues. Vascularized liver spheroids were described in the context of liver cancer using a hanging-drop method to allow interaction between HepG2 and human umbilical vein endothelial cells (HUVECs) [13].

---

Flavio Bonanini, Dorota Kurek, Sara Previdi have contributed equally to this study.

✉ Paul Vulto  
p.vulto@mimetas.com

<sup>1</sup> Mimetas, Leiden, The Netherlands

<sup>2</sup> Oncode Institute, Hubrecht Institute, Royal Netherlands Academy of Arts and Sciences and University Medical Center, 3584 CT Utrecht, The Netherlands

<sup>3</sup> The Maastricht Multimodal Molecular Imaging Institute, Maastricht University, Maastricht, The Netherlands

Subsequently, Inamori et al. demonstrated the possibility to vascularize primary hepatocyte spheroids by an endothelial cell encapsulation method [14]. Another approach included the generation of liver tissue using a layer-by-layer cell coating technique of hepatocytes, dermal fibroblasts, and HUVECs [15]. Others generated multicellular tissue constructs combining induced hepatic cells and HUVECs in decellularized liver scaffolds [16]. Although functional for studying cell–cell interaction, these methods did not yield stable, accessible, let-alone perfusable, microvascular networks. Alternatively, transplantation of spheroids/organoids into highly vascularized sites in mice allows vascularization of microtissues by the host [17] resulting in improved liver maturation and functionally [18, 19]. Although functionally powerful, xenografting has limited scalability and suffers from limited success rates and reproducibility. Moreover, the high cost, limited accessibility, and increasing ethical pressure limit the routine adoption of xenografting into laboratory practice [20].

Organ-on-a-chip technology is a promising tool to aid advanced tissue culture, as it can provide perfusion flow, gradients, and structured layering of tissues [21]. In a typical setup, two microfluidic channels are divided by a permeable membrane to separate the endothelial and hepatic compartments [22]. These chips have been shown to be advantageous for disease induction, liver zonation [23], and studying species-specific toxicity [24]. Direct interaction between a vascular network and a tissue of interest has been studied in a range of microfluidic setups, utilizing either vasculogenesis or angiogenesis approaches in hydrogel-supported cultures [25–27]. In order to accommodate the interaction of larger target tissues with microfluidic grown vasculature, so-called “open-top” chips were introduced [28]. For example, Oh et al. developed an open-top microfluidic chip in which microvasculature grown in a microfluidic network was allowed to interact with tumor cells placed on top of a porous membrane [29]. Nashimoto et al. utilized a micropillar approach to assess the angiogenic potential of mixed fibroblast-tumor spheroids, leading to juxtacrine interaction with vascular sprouts [30, 31]. Linn et al. developed a system of three communicating wells of a 384-well plate, in which mixed HepG2 spheroids, endothelial cells, and fibroblasts resulted in the self-organization of a perfusable 3D vascular network [32].

Notwithstanding this substantial progress, there is a need for a readily available platform that allows for routine vascularization of tissues *in vitro*. Here, we introduce a platform, dubbed the OrganoPlate Graft, comprising 64 microfluidic chips underneath a microtiter plate. Each chip allows for establishing a vascular bed through induction of angiogenesis from two main endothelial vessels. A target tissue is placed on top of the vascular bed for subsequent vascularization. We demonstrated vascularization of hepatic

spheroids and organoids and perfusion of resulting microvascular networks. We further demonstrated the possibility to model veno-occlusive disease (VOD), an endothelial damage-associated disease in a liver context, upon exposure to azathioprine [33–37]. We foresee the use of the platform for *in vitro* grafting of a broad range of tissues, ultimately replacing animal grafting.

## Materials and methods

### Cell culture

Human primary RFP-labeled HUVECs (Alphabioregen, #RFP4) were cultured in T75 flasks (Corning, #734–2705) in MV2 (PromoCell, #C-22121) supplemented with 1% penicillin/streptomycin (Sigma, #P4333) and used at passage 4 till passage 8 for all experiments. Before use, a T75 flask was pre-coated with 50 µg/mL Purecol (Advanced BioMatrix, #5005-B) for 30 min at 37 °C in PBS (phosphate-buffered saline, Life tech #20,012,068) and then washed twice with sterile PBS. Cryopreserved Upcyte® Human Hepatocytes (UHH) from donor 653–03 were purchased from Upcyte technologies GmbH (Hamburg, Germany) and cultured as previously described [38]. Briefly, UHH were thawed in Thawing Medium (Upcyte technologies, #MHE001) seeded at a density of 10,000 cells/cm<sup>2</sup> in collagen-type I-coated T75 flasks (Thermo, #156,499) and cultured in High-Performance Medium (HPM, Upcyte technologies, #MHE003). Media were replaced three times a week. All cells regularly tested negative for mycoplasma. For all cells, culture was performed in a humidified incubator at 37 °C and 5% CO<sub>2</sub>.

### Spheroids and organoids generation

To form hepatic spheroids, UHH at 100% confluency was dissociated using TrypLE™ Express Enzyme (Thermo, #12,604,021), and viability was assessed using the trypan blue dye exclusion method. 100 µl of HPM containing 20,000 UHH cells was transferred into each well of a Costar® ultra-low attachment 96-well plate (Corning, #CLS3474-24EA) and centrifuged for 1 min at 100 × *g*. For pre-vascularized spheroids, a mix of 1000 RFP-labeled HUVECs and 20,000 UHH were used. The plate was then placed in a humidified incubator (37 °C and 5% CO<sub>2</sub>). After 48 h, the spheroids were transferred onto the OrganoPlate Graft. Human hepatic organoids were generated from human fetal tissue as previously described [39]. After that, hepatic organoids were dissociated to single cells, and 6000 hepatocytes were added to each well of a Costar® ultra-low attachment 96-well plate in 100 µl of human Hep-Medium [39] and centrifuged for 5 min at 100 × *g*. After 3 days, organoids were transferred to the OrganoPlate Graft.

## Microfluidic cell culture

OrganoPlate culture was performed using the OrganoPlate Graft with 400  $\mu\text{m} \times 220 \mu\text{m}$  ( $w \times h$ ) channels (Mimetas BV, the Netherlands). Phaseguides had dimensions of 100  $\mu\text{m} \times 55 \mu\text{m}$  ( $w \times h$ ). Gel and perfusion channels had a length of 9 mm and 13 mm, respectively, with a downstream phaseguide wall interface of approximately 132 and 164 degrees. The phaseguide stability is expected to be around 200 Pa [40]. 2.5  $\mu\text{l}$  of gel composed of 4 mg/ml Collagen I (AMSBio Cultrex 3D Collagen I Rat Tail, 5 mg/ml, #3447–020-01), 100 mM HEPES (Life Technologies, #15,630–122), and 3.7 mg/ml  $\text{NaHCO}_3$  (Sigma, #S5761) was dispensed in the gel inlet and incubated 15 min at 37 °C. Endothelial cells were detached by use of TrypLE™ Express Enzyme (Thermo, #12,604,021), counted and pelleted (5 min, 300  $\times g$ ). The cells were applied to the system by seeding 2  $\mu\text{l}$  of  $1 \times 10^7$  of cells/ml in the inlets of the perfusion channels. Subsequently, 50  $\mu\text{l}$  of MV2 medium was added to the same inlets and the OrganoPlate was incubated in humidified conditions at 37 °C and 5%  $\text{CO}_2$  for at least 1 h until cells attached on the bottom of the perfusion channels. After incubation, 50  $\mu\text{l}$  medium was added to both channel outlets. The OrganoPlate was placed in the incubator (37 °C and 5%  $\text{CO}_2$ ) on an interval rocker switching between a + 14° and – 14° inclination every 8 min (OrganoFlow S, Mimetas) allowing bi-directional flow. Medium (50  $\mu\text{l}$  each on inlet and outlet) was refreshed every 2–3 days. Endothelial tubes were cultured for 2–3 days before inducing microvascular bed formation.

## Microvascular bed formation

Sprouting of RFP-labeled HUVEC was induced by addition to the graft chambers of 50  $\mu\text{l}$  of MV2 medium containing angiogenic factors: 50 ng/ml vascular endothelial growth factor (VEGF), 20 ng/ml basic fibroblast growth factor (bFGF), 2 ng/ml Phorbol 12-myristate 13-acetate (PMA), and 500 nM Sphingosine 1-phosphate (S1P). Stock solutions were prepared as follows: 100  $\mu\text{g/ml}$  murine VEGF in MilliQ water (Peprotech, #100–20), 50  $\mu\text{g/ml}$  bFGF in MilliQ water (Peprotech, #G00832 100-18B), 1 mM S1P (Sigma, #G00918) in 5% 1 M HCl, 95% DMSO, 10  $\mu\text{g/ml}$  PMA (Sigma, # P1585) in 1% DMSO, and 100  $\mu\text{g/ml}$ . Sprouting mix was refreshed every 2–3 days.

## Microvessels characterization

To measure microvessels area and orientation, the microvascular bed was stained with Calcein AM green (Life Technologies, #C3099, 1:2000) in MV2 medium. After incubation for 30 min in the incubator (37 °C and 5%  $\text{CO}_2$ ) on an interval rocker switching between a + 14° and – 14° inclination

every 8 min (OrganoFlow S, Mimetas), maximum intensity projections were acquired using the Micro XLS-C High Content Imaging Systems (Molecular Devices, US) at 4 $\times$  magnification. Maximum intensity projections from each chip were used to calculate the average microvessel orientation and microvessel area using the ‘orientationJ analysis’ tool and a modified version of the ‘morphology’ plugin in FIJI v.1.52. Data underlying Fig. 1f, e were obtained making use of automated image analysis routines that are described in supplementary Fig. 1c.

## Hepatic microtissue culture with microvessels

After 4–5 days of endothelial cell sprouting, hepatic microtissues were placed in the circular opening in the graft chamber on top of the microvascular bed. Before microtissue placement, medium was refreshed as follows: for hepatic spheroids, medium was aspirated from all graft chambers, in- and outlets and replaced with 50  $\mu\text{l}$  MV2 (in- and outlets) and 50  $\mu\text{l}$  HPM (graft chamber); for hepatic organoids, medium was aspirated from all graft chambers, in- and outlets and replaced with 50  $\mu\text{l}$  Hep-Medium (in- and outlets). Graft chamber was left dry to allow overlay of organoids with Matrigel.

For manual placement of hepatic spheroids, microtissues were picked up from the ultra-low attachment plate together with 20  $\mu\text{l}$  culture medium using wide-bore tips (Pure™ 200G Pipet Tips, VWR, #53,225–682). The pipette tip was then placed above the circular opening of the graft chamber allowing the spheroid to slowly sediment from the pipette tip onto the microvascular bed. For placement with liquid handler, the same procedure was followed using the OT-2 robot (Opentrons). Position accuracy of the spheroids for both manual and automated placement was determined by measuring the relative position along XY axis versus the center of the graft chamber using FIJI v.1.52 and translating to a radial offset. The OrganoPlates were then placed in the incubator (37 °C and 5%  $\text{CO}_2$ ) and were kept static for 1 h to allow the spheroids to adhere to the underlying collagen-I matrix. This prevents displacement during initial stages of rocking as well as during subsequent medium changes.

Hepatic organoids were transferred manually using a standard p10 micropipette into the circular opening in the graft chamber. After placement, 5  $\mu\text{l}$  Matrigel GFR (Corning, #356,231) was added on top of each organoid, and the gel was allowed to polymerize for 10 min at 37 °C. At the end of the incubation, 50  $\mu\text{l}$  Hep-Medium was added to all graft chambers.

The OrganoPlates were then placed on an interval rocker switching between a + 14° and – 14° inclination every 8 min (OrganoFlow S, Mimetas) allowing bi-directional flow. Media were refreshed every 2–3 days.

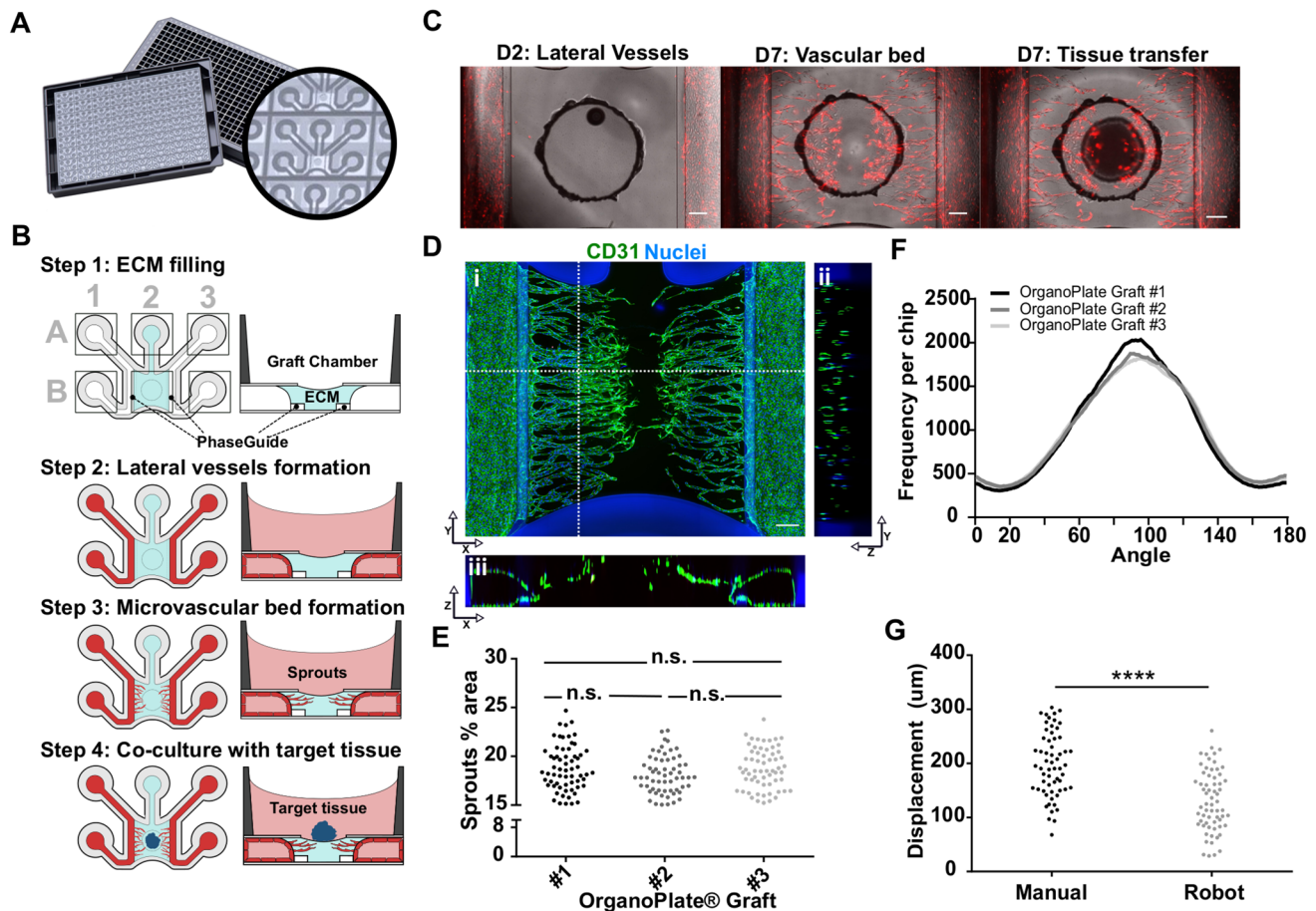


**Fig. 1** The OrganoPlate Graft allows for the generation of robust microvascular beds. **a** Top and bottom views of the OrganoPlate Graft with 64 microfluidic units positioned underneath a 384 microtiter plate. Each microfluidic unit makes use of a  $2 \times 3$  array of wells from the microtiter plate (insert image). **b** Sequence of steps for generating a microvascular bed. Step 1: the graft chamber is filled with Collagen I gel (depicted in blue) through the gel inlet A2. Step 2: endothelial cells are seeded against collagen I gel (depicted in red) in the two lateral perfusion channels and form tubules upon application of perfusion flow. Step 3: Angiogenic factors are added to the graft chamber B2 to induce sprouting of the lateral vessels and formation of the vascular bed. Step 4: once microvessels have reached the opening on the graft chamber, a target microtissue is positioned on top of the microvascular bed to initiate interaction. **c** Images of an RFP-labeled HUVEC vascular bed formation prior to application of angio-

genic factors (left) and after (middle). The target tissue is then positioned on the center of the graft chamber opening (right). Scale bar: 200  $\mu\text{m}$ . **d** Maximum intensity projection (i) and cross sections (ii, iii) of a microvascular bed stained against CD31 (green) and nuclei (blue). Microvessels with a lumen are apparent. Location of cross sections is indicated by dash lines. Scale bars: 200  $\mu\text{m}$ . **e** Quantification of sprout area coverage in 64 microfluidic units per OrganoPlate for three different plates ( $n = 192$ ) after microvascular bed formation. Significance was calculated using one-way ANOVA and shown as non-significant (ns,  $P > 0.05$ ). **f** Average distribution frequency of the orientation of microvascular structures (90 degrees indicates horizontal alignment) from 3 different OrganoPlate Grafts. **g** Evaluation of manual and robotic placement accuracy of target tissue on top of the microvascular bed. Statistical significance was attributed to values of  $P < 0.05$  as determined by unpaired Student's *t* test

### Quantification of vessel intensity over time

Fluorescent images were acquired every 2–3 days using an ImageXpress XLS Micro High content imaging system at 37 °C ( $4 \times$  objective). FIJI v.1.52 was used to quantify the relative RFP-HUVEC vessel intensity by drawing a rectangular selection excluding the lateral perfusion channels and measuring the mean signal intensity.

### Barrier integrity assay

Barrier integrity of lateral vessels was examined by addition of MV2 media containing 0.5 mg/ml FITC-dextran (150 kDa, Sigma #46,946) to both perfusion channels (40  $\mu\text{l}$  in the inlets and 20  $\mu\text{l}$  in the outlets). 20  $\mu\text{l}$  of fresh media without dye was added to the graft chamber. Images were acquired every 15 s for 8 min using an

ImageXpress XLS Micro High content imaging system at 37 °C (4× objective).

## Immunohistochemistry

For direct immunostaining in the OrganoPlate Graft of co-cultures, cells were fixed with 3.7% formaldehyde (Sigma, #252,549) in PBS (phosphate-buffered saline, Life tech #20,012,068) for 15 min. After washing twice for 5 min with PBS, permeabilization and blocking were carried out together using 0.3% Triton X-100 (Sigma, #T8787), 2% FCS, 2% bovine serum albumin (BSA) (Sigma, #A2153), and 0.1% Tween 20 (Sigma, #P9416) in PBS for 2 h. Subsequently, cells were incubated with primary antibodies overnight, washed three times, incubated with secondary antibodies for 2 h, and washed three times with 4% FCS in PBS. The following antibodies were used for immunohistochemistry: Mouse a-CD31 (Dako, M0823, Clone JC70A, 1:20), Goat a-Albumin FITC conjugated (Bethyl, A80-229F, 1:200), Mouse a-HNF4A (Thermo Fisher, MA1199, 1:500), Mouse a-MRP2 (Abcam, M2 III-6, ab3373, 1:100), Mouse a-acetylated tubulin (Sigma, T6793, 1:4000) Mouse a-E-cadherin (BD, 610,181, 1:300), and Goat a-Mouse AlexaFluor 647 (Thermo Fisher, #A31571, 1:250). After nuclear stain with Hoechst (Thermo Fisher Scientific, #H3570, 1:2000 in PBS) cells were stored in PBS (50 µl in all graft chambers and in- and outlets). Tissue clearing was performed using CUBIC reagents (TCI Chemicals, Cubic-L, and CUBIC-R+) according to manufacturer instructions.

All steps were performed at room temperature (RT) and under the presence of flow. Cells were imaged with the EVOS FL2 Auto, ImageXpress Micro XLS, and Micro XLS-C High Content Imaging Systems (Molecular Devices, US).

For immunostaining of hepatic spheroids sections, vascularized spheroids were first removed from the graft chamber at different timepoints of the co-culture, transferred to cryomolds, overlaid with Cryo-Gel (Leica, #39,475,237) and frozen by floating in an ethanol/dry ice bath. After solidification, cryomolds were stored at –80 °C until cryosectioning. Cryosectioning was performed using a cryostat (Cryotome® FE, Thermo Scientific) at –20 °C. 10 µm cryosections were collected on SuperFrost® Plus slides (Fisher Scientific, #10,149,870). The slides were air-dried and fixed with 3.7% formaldehyde (Sigma, #252,549) in PBS for 15 min. After washing twice for 5 min with PBS, sections were permeabilized with 0.5% Tween in PBS for 10 min and blocked with 2% BSA and 0.05% Tween in PBS. Sections were incubated with Mouse a-CD31 (Dako, M0823, Clone JC70A, 1:20), Goat a-Albumin FITC conjugated (Bethyl, A80-229F, 1:200) for 2 h, washed three times 5 min with washing solution (0.05% Tween in PBS) and incubated with secondary antibody for 1 h. After washing three times, nuclei were

stained with DAPI (Thermo Fisher Scientific, #R37606). Sections were mounted with Vectashield (Vector Laboratories, #H-1400) and imaged with EVOS FL2 Auto.

## Perfusion assay

Interconnection and perfusion between the left and right side of the vascular network in the presence of microtissues were determined by addition of 100 µl MV2 medium containing 0.25 mg/ml FITC-Dextran (150 kDa, Sigma #46,946) to the left perfusion inlet, while 50 µl of MV2 medium was added to the left perfusion outlet and right in- and outlets. Medium in the Perfusion channels was removed for the course of the assay. Images were acquired every 60 s for 5 min using an ImageXpress XLS Micro High content imaging system at 37 °C (4× objective). Perfusability of the vascular network was identified, when perfusion with fluorescent dye was observed via the lumen of vascular network from the left channel to the right perfusion channel. Perfusable chips were identified manually, when apparent flow of the dye was observed to traverse the vascular network reaching the right perfusion channel.

## Transmission electron microscopy

A co-culture of hepatic organoids with vascular bed was fixed with 1.6% glutaraldehyde for 24 h at 4 °C and removed from the OrganoPlate. Then, samples were kept in wash buffer (0.1 M cacodylate) until further processing. Samples underwent an additional fixation step with 1% osmium tetroxide and 1.5% potassium ferricyanide in wash buffer for 1 h in the dark at 4 °C. Further, the samples were progressively dehydrated in ethanol 70–100% and infiltrated with Epon resin for 2 days. Then, samples were embedded in Epon resin, which polymerized for 2 days at 60 °C. Ultrathin sections were cut using an ultramicrotome (Leica Ultracut UCT) and mounted on Formvar-coated copper grids. Sections were stained with 2% uranyl acetate in water and lead citrate. Sections were imaged using a Tecnai T12 electron microscope and an Eagle 4 k\*4 k CCD camera (ThermoFisher Scientific).

## Bile canaliculi staining

Staining with CDFDA was performed to visualize active bile canaliculi in the hepatic organoids co-cultured with microvessels. Briefly, a stock solution containing 5 mM 5-(and-6)-carboxy-2',7'-dichloro-fluorescein diacetate (CDFDA) (Sigma-Aldrich, #2188) was prepared in 100% Dimethyl Sulfoxide (DMSO) (Sigma, #D8418), aliquoted, and stored at –20 °C. For the assay, culturing media were aspirated in all graft chambers and perfusion in- and outlets and 50 µL of Hep-Medium containing 5 µM CDFDA

(1:1000), and Hoechst (Thermo Fisher Scientific, #H3570, 1:2000 in PBS) was added to each well. The OrganoPlate Graft was incubated for 30 min in the incubator (37 °C, 5%, CO<sub>2</sub>) on an interval rocker switching between a +14° and -14° inclination every 8 min (OrganoFlow S, Mimetas). As negative control, Hep-Medium media containing 0.1% DMSO and Hoechst (Thermo Fisher Scientific, #H3570, 1:2000 in PBS) was prepared. At the end of the incubation, chips were washed 6 times with PBS and imaged Micro XLS-C High Content Imaging Systems (Molecular Devices, US).

### Functional analysis of hepatic spheroids and organoids

To determine the levels of albumin secreted over time by spheroids and organoids, co-culture media were collected from perfusion channels and graft chambers (day 3, 5, and 7 for spheroids, day 7, 14, and 21 for organoids) and analyzed using the Human Albumin ELISA Quantification kit (Bethyl Laboratories Inc., E80-129, sample dilution 1:125).

Urea production was determined by a colorimetric assay kit (Biovision, #K375-100, sample dilution 1:5) following the manufacturer's protocol.

### Viability determination

For this experiment, vascular beds were formed using HUVECs (Lonza, #2519AS) using a modified concentration of S1P (250 nM) and PMA (10 ng/ml), and endothelial cells were sprouted for 3 days. Spheroids were composed of 7500 UHH from donor 151–03. AZA was administered in both, perfusion lanes and graft chamber at a concentration range from 0.66 μM to 160 μM for 72 h (days 2–5 of co-culture with microvessels). CellTiter Glo3D (Promega, #G9681) was used to determine the toxic effect of Azathioprine on liver cultures. For this, medium was aspirated from all wells and replaced with 50 μl of a 1:1 mixture of CellTiter Glo3D reagent and Hanks' Balanced Salt Solution (HBSS, Gibco #14,025,092). The plate was then shaken for 15 min at 300 rpm (1 mm displacement) to lyse the cells and initiate the light reaction. 24 μl of the lysate was transferred to a white 384-well plate and luminescence was recorded. Luminescence was measured from lysate in graft chambers and perfusion lanes separately. Relative luminescence units were normalized to untreated condition which was defined 100% viable.

### Azathioprine exposure

After 5 days of co-culture, vascularized spheroid co-cultures were exposed to 50 μM Azathioprine (Sigma-Aldrich, PHR1282) or to vehicle control (0.1% DMSO). 50 μl of 50 μM Azathioprine or vehicle control was added to all

perfusion channels in-and outlets (in MV2 medium) and to the graft chamber (in HPM medium), and the plates were placed back in the incubator on an interval rocker switching between a +14° and -14° inclination every 8 min (OrganoFlow S, Mimetas). After 48 h, medium was collected for LDH quantification, and the perfusion assay was performed. Subsequently, medium was removed, and 5 μM of SytoX™ Green Nucleic Acid Stain (Thermo Fisher Scientific, #S7020) in MV2 was added to all perfusion channel in- and outlets and to the graft chamber for 15 min. Dead cells were visualized using a ImageXpress XLS Micro High content imaging system at 37 °C (4× and 10× objective). Dead nuclei quantification was performed using FIJI v.1.52 by thresholding cropped images (removing the lateral perfusion channels) using the “default” algorithm followed by “watershed” and “analyze particles.” LDH release was performed using LDH™-Glo cytotoxicity assay (Promega, #J2380, sample dilution 1:75) according to the manufacturer's instructions.

### Statistical analysis

Statistical analysis was done in GraphPad Prism 8 (GraphPad Software, USA), and statistical significance was attributed to values of  $P < 0.05$  as determined by Student's *t* test or two-way ANOVA analysis, as described in the figure legends. Data are expressed as mean ± SD or SEM as described in the figure legends.

## Results

### The OrganoPlate Graft allows for the generation of robust microvascular beds

The OrganoPlate Graft consists of 64 microfluidic chips patterned underneath a standard 384-well plate (Fig. 1a). Each chip comprises two perfusion channels and a gel channel, which are connecting six wells per chip (Fig. 1a). The perfusion channels and gel channel join in a central chamber, called the graft chamber (Fig. 1b). The graft chamber has an opening at the top that allows placement of a target tissue. Two phaseguides [40, 41] on the bottom surface of the microfluidic layer allow filling the graft chamber with an extracellular matrix (ECM) gel. Phaseguides are small ridges at the bottom of a microfluidic channel that act as capillary pressure barriers for an advancing liquid–air meniscus. In this manner, a liquid ECM gel precursor can be added to the graft chamber without overflowing into the adjacent perfusion channels. The use of surface tension techniques for ECM patterning obviates the need for artificial membranes in creating a layered culture setup [41, 42]. In this study, we exclusively

utilized collagen I to pattern the microfluidics; however, several different ECM gels have been reported in conjunction with phaseguide technology [43–45]. The process of in vitro tissue grafting consist of four main steps, as illustrated in Fig. 1b: First, a collagen-I gel precursor is dispensed into the gel inlet (A2 in Fig. 1b) with subsequent gelation for 15 min at 37 °C. Next, RFP-expressing human HUVECs are introduced in the lateral perfusion channels (inlets A1 and A3 in Fig. 1b). Once cells settled and attached to the bottom of the channel, gravity-driven perfusion was initiated by placing the plate on an interval rocker (Supplementary Fig. 1a). After three days of culture, two confluent endothelial tubules (here called lateral vessels) were formed in the perfusion channels with lumen that are accessible from the in- and outlets (A1, B2, and A3, B3 in Fig. 1b). As a third step, a cocktail of four angiogenic factors is added to the graft chamber (B2 in Fig. 1b). The combination of VEGF, S1P, PMA, and bFGF induced sprouting of the endothelial vessels into the adjacent collagen-I gel with a tip-stalk cell hierarchy, typical for the angiogenesis process [46]. After four days of exposure to the angiogenic factors, a microvascular bed was formed with microvessels spanning the length from the lateral vessels to the graft chamber opening (Fig. 1c and Supplementary Video 1). As a last step, angiogenic factors are removed and a target tissue is placed in the graft chamber on top of the microvascular bed (Fig. 1c). Figure 1d shows a microvascular bed that was stained for the endothelial marker CD31 in combination with a nuclear stain, including a reconstruction of a cross section orthogonal ( $y-z$ ) and parallel ( $x-z$ ) to the sprouting direction. Cross sections reveal that microvessels have a lumen and penetrate the collagen toward the opening of the graft chamber. To characterize the reproducibility of vascular bed formation between chips and plates, we assessed variation of 64 vascular beds in three independent plates (Supplementary Fig. 1b, c). Coverage of the microvascular bed area as a percentage of the total surface area showed low chip-to-chip and plate-to-plate variations (Fig. 1e) with average coverage of  $18.4 \pm 2.2\%$  (SD). No difference was observed between the three plates. Sprouting of microvessels toward the graft chamber occurred radially toward the graft chamber opening, with  $40.19 \pm 1.6\%$  (SD) of structures falling between  $80.5^\circ$  and  $100^\circ$  (Fig. 1f). Orientation was defined with respect to the longitudinal direction of the phaseguide and lateral perfusion channels. Upon removal of angiogenic factors, pre-formed hepatocyte spheroids (Supplementary Fig. 2a) were transferred from low attachment plates to the graft chamber (Fig. 1c). The spheroids were placed on top of the microvascular bed either manually or using a pipetting robot (Supplementary Fig. 2b and c and Supplementary Video 3). Robot-operated tissue placement provided better centering of the tissue

compared to manual transfer (Fig. 1g) with an average displacement of  $131 \pm 56.2 \mu\text{m}$  (SD) with respect to the center of the inlet compared to manual positioning displacement of  $198 \pm 59.2 \mu\text{m}$  (SD).

### Vascular remodeling is induced by hepatic microtissues

The interaction of a hepatic spheroid with the pre-formed microvascular bed was assessed. Microvascular beds were formed from RFP-HUVECs, as described before. After four days of angiogenesis, the sprouting cocktail in the graft chamber was replaced with HPM. Lateral perfusion channels were supplied with MV2 medium. Hepatocyte spheroids comprising of 20,000 hepatocytes were placed in the graft chamber, on top of the collagen matrix hosting the microvascular bed and the co-culture was maintained for 7 days (Supplementary Video 2) with medium changes every 2–3 days. Figure 2a shows images of the vascular bed and Fig. 2b the quantification of the area covered by RFP-HUVEC vascular bed in the graft chamber with and without the addition of a hepatocyte spheroid upon removal of angiogenesis factors at day 7. In the presence of a spheroid, microvasculature was maintained over the co-culture period of 7 days, whereas in its absence, the microvascular bed underwent pruning, resulting in an almost complete retraction of the microvessels. Interestingly, when no sprouting cocktail was used, the presence of the spheroid alone was sufficient for inducing sprouting after 7 days of co-culture (Supplementary Fig. 3a and b). These results indicate that hepatocyte spheroids possess high angiogenic potential and support existing microvasculature. To confirm maintenance of hepatic function during co-culture, we assessed release of albumin. Figure 2c shows a similar trend in albumin secretion over time for spheroids in the presence or absence of a vascular bed. However, we observed a generally lower albumin release when spheroids were co-cultured with microvessels. Still, we can conclude that hepatic function was maintained in a vascularized context over the period of co-culture. Co-culture with spheroids also appears to increase barrier integrity of the lateral vessels, where we observed reduced FITC-dextran leakage in the graft chamber opening and the surrounding gel (Supplementary Fig. 4). We then investigated hepatic organoids as an alternative hepatocyte source. Hepatic organoids have been established by Hu et al. using mouse and primary human hepatocytes [47]. These organoids have been reported to allow expansion for multiple months while maintaining key morphological features and hepatic functionalities. Moreover, these human hepatocyte organoids maintain remarkable regenerative capacity, as shown by extensive proliferation after engraftment into mice [47]. Here, human hepatic organoid aggregates of uniform size and shape (Supplementary

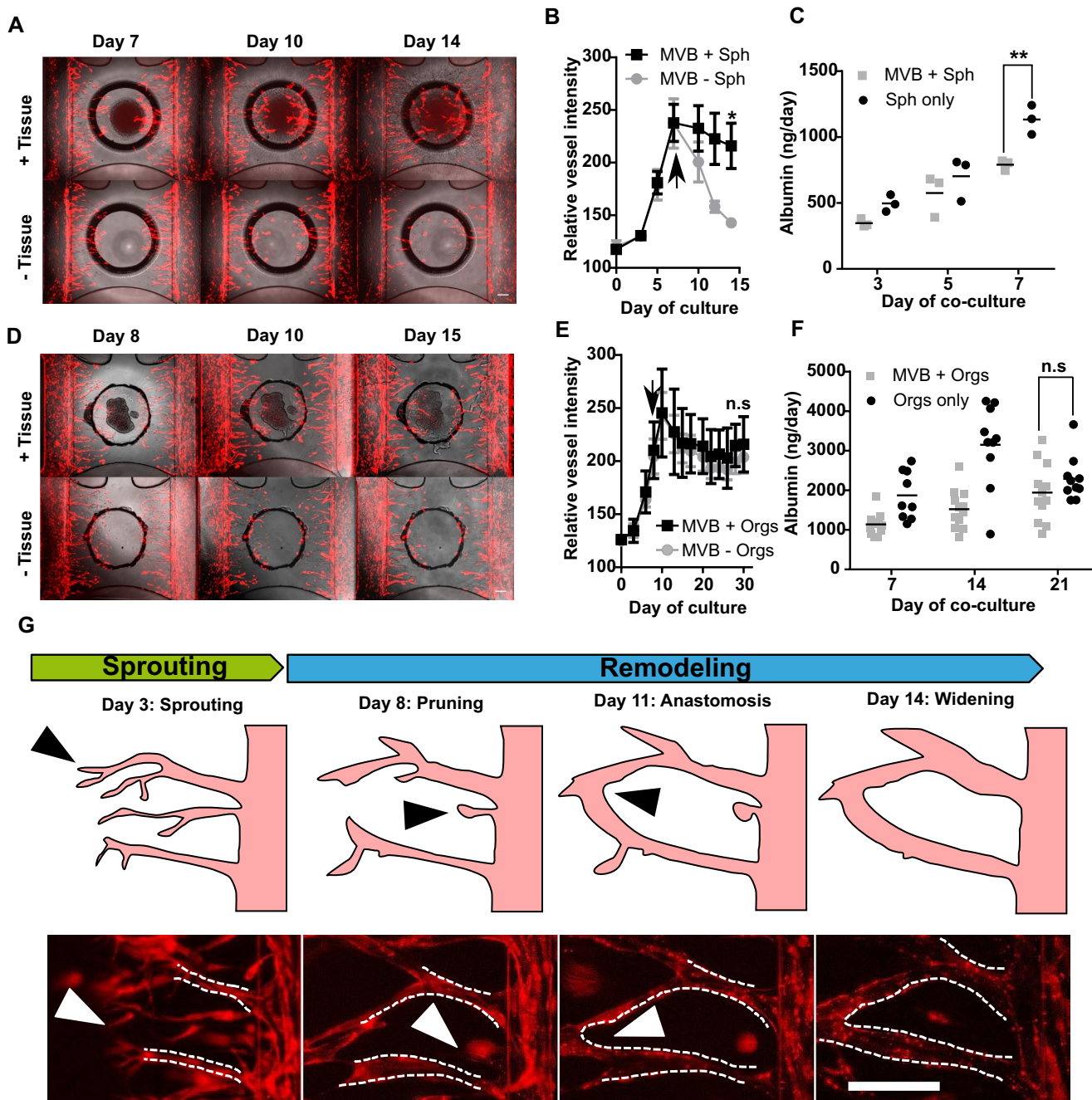


Fig. 5a) were transferred to the OrganoPlate Graft on top of pre-formed microvascular beds. In contrast to hepatocyte spheroids, which were directly exposed to the medium in the graft chamber, hepatocyte organoids were additionally overlaid with a Matrigel droplet (Supplementary Fig. 5b). Upon tissue placement, medium in the graft chamber was replaced with Hep-medium while MV2 medium was kept in the perfusion channels. Figure 2d shows images of the vascular bed with and without grafted organoids, Fig. 2e quantification of the vascular bed area, and Fig. 2f albumin release over the culture period of 30 days (corresponding

to 21 days of co-culture). Similar as for hepatocyte spheroids, microvasculature integrity was maintained when co-cultured with hepatic organoids (Fig. 2d). However, we did not observe a regression of the vasculature in absence of the organoids, possibly because the growth factors in Hep-medium were sufficient for stabilizing the microvasculature (Fig. 2e). To confirm this, we cultured microvascular beds in basal Hep-medium in the graft chamber supplemented with either HGF, FGF10 or EGF at concentrations previously described [44] and we observed that HGF alone was capable of stabilizing the vascular structures over a period of

**Fig. 2** Vascular remodeling is induced by hepatic microtissues. **a** Phase-contrast images with fluorescence overlay of hepatocyte spheroids grafted on top of a microvascular bed (top panel) in comparison to a microvascular bed only (bottom panel) at day 7, 10 and 14 of culture which represent day 0, 3, and 7 of co-culture. Scale bar: 200  $\mu$ m. **b** Relative microvascular bed (MVB) RFP signal in presence (black squares) or absence (gray circles) of hepatocyte spheroids (Sph) during 14 days of culture. Spheroids were transferred at day 7 of culture as indicated by the black arrow. Data represents mean  $\pm$  SD,  $n=8-16$ , statistical significance was attributed to value of  $*P<0.01$  as determined by unpaired Student's *t* test on day 14 timepoint. **c** Albumin secretion of hepatocyte spheroids during 7 days of co-culture in the presence (gray squares) or absence (black circles) of a microvascular bed. Dots represent individual chips, line represents mean,  $n=3$ , statistical significance was attributed to value of  $**P<0.001$  as determined by unpaired Student's *t* test on day 14 timepoint. **d** Phase-contrast images with fluorescence overlay of hepatic organoids grafted on top of a microvascular bed (top panel) in comparison to a microvascular bed only (bottom panel) at day 8, 10 and 14 of culture which represent day 0, 2 and 6 of co-culture. Sale bar: 200  $\mu$ m. **e** Relative microvascular bed (MVB) RFP signal in the presence (black squares) or absence (gray circles) of hepatic organoids (orgs) during 30 days of culture. Organoids were transferred at day 8 of culture as indicated by the black arrow. Data represent mean  $\pm$  SD,  $n=8-14$ , significance was calculated by unpaired Student's *t* test on day 30 timepoint and shown as non-significant (n.s.,  $P>0.05$ ). **f** Albumin secretion of hepatocyte organoids during 21 days of co-culture in the presence (gray squares) or absence (black circles) of a microvascular bed. Dots represent individual chips, line represents mean,  $n=5-9$ , significance was calculated by unpaired Student's *t* test on day 21 timepoint and shown as non-significant (n.s.,  $P>0.05$ ). **g** Angiogenesis process of RFP-labeled HUVEC during initial sprouting and subsequent vascular structures remodeling in the presence of a hepatocyte spheroid from day 7 of culture. Pictures show filopodia (left, white arrow), microvessel retraction (middle left, white arrow), anastomosis (middle right, white arrow) and widening (right). Scale bar: 200  $\mu$ m

6 days (Supplementary Fig. 6). Similar to hepatocyte spheroids, barrier integrity of the lateral vessels appeared to be increased when organoids were co-cultured with microvessels (Supplementary Fig. 4). A hepatic phenotype was maintained during the culture period, as indicated by albumin release (Fig. 2f), expression of hepatocyte nuclear factor 4 alpha (HNF4 $\alpha$ ), acetylated tubulin (Ac. Tub) and E-cadherin (ECAD) (Supplementary Fig. 5c). Furthermore, hepatic organoids incubated with the fluorescent compound 5-chloromethylfluorescein diacetate (CMFDA) showed functionality and polarization of the canalicular MRP2 transporter (Supplementary Fig. 5d) and were capable of producing and secreting urea throughout the 21 days of co-culture (Supplementary Fig. 5e).

During the vascularization process of hepatocyte spheroids, the endothelial vessels undergo all stages typical of the angiogenesis process (Fig. 2g). HUVECs migrate and elongate toward the graft chamber with a clear presence of filopodia in tip cells leading the emerging microvessels (Fig. 2g, left). Upon removal of angiogenic factors and placement of the hepatic spheroids, non-connected sprouts undergo pruning (Fig. 2g, middle left), whereas others

undergo anastomosis (Fig. 2g, middle right) and show overall widening of microvascular structures (Fig. 2g, right). As a result of this extensive remodeling, a vascular structure emerges with distinct, spatially separated afferent vessels that developed orthogonally from the lateral vessels toward the hepatic spheroids.

### Endothelial cells penetrate hepatic microtissues forming lumenized, perfusable microvasculature

Figure 3a, b respectively shows vascularized spheroids and organoids resulting from 7 days (spheroids) and 21 days (organoids) of co-culture with microvessels stained for CD31 and albumin. Confocal imaging revealed the presence of lumenized spaces in the afferent vessels connecting the spheroid with the lateral vessels (Fig. 3c, i) and in smaller vessels in close proximity to hepatocytes (Fig. 3c, ii, Supplementary Fig. 3c). We observed the presence of microvascular structures at different depths throughout the hepatic spheroids (Supplementary Fig. 7a and Supplementary Fig. 7b). To further validate whether microvascular remodeling leads to penetration of microvessels in the hepatic microtissues, hepatocyte spheroids were co-cultured with microvascular beds and extracted after 1, 4 or 7 days followed by cryosectioning and immunostaining for CD31 and Albumin. At day 4, endothelial cells appeared to superficially interact with hepatocyte spheroids (Fig. 3d, ii). At day 7, however, endothelial cells penetrated the hepatocyte spheroids (Fig. 3d, iii). Vessel lumen was confirmed by TEM imaging (Fig. 3e, i) which also revealed that vessels in direct contact with hepatic organoids showed the presence of pinocytotic vesicles, suggesting transport through the vascular wall as well as ECM deposition (Fig. 3e, ii). Next, we assessed whether the vascular network could be perfused with a 150 kDa FITC-labeled dextran. A hydrostatic pressure difference was applied between the inlets connecting the left and right lateral vessels, forcing the fluorescent molecules through the microvascular bed (Fig. 3f and Supplementary Fig. 7c). Indeed, it was possible to observe a flux of fluorescent dye from one lateral vessel through the microvascular network and the spheroid into the other lateral vessel on the opposite side (Fig. 3g). For organoids, we were not able to observe complete interconnection (data not shown). Despite not detrimental for vascular structures, hepatic organoids in this context were not capable of significantly promoting further vascular structures remodeling as hepatic spheroids were.

### Modeling veno-occlusive disease

Azathioprine (AZA) is an immunosuppressive agent used in organ transplantation to prevent rejections. It is associated with veno-occlusive disease (VOD), also known

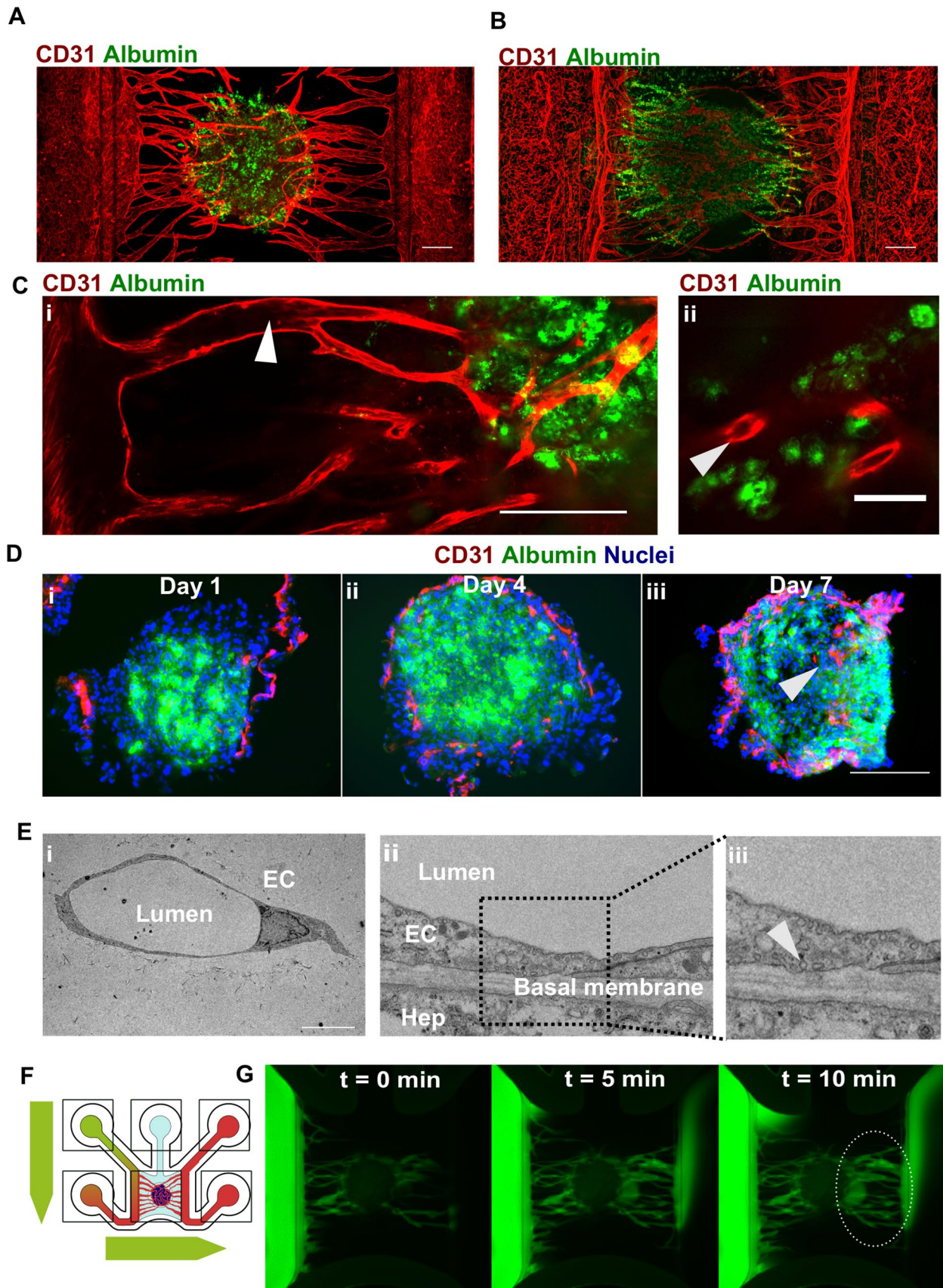


**Fig. 3** Endothelial cells penetrate hepatic microtissues forming lumenized, perfusable microvasculature. **a** Maximum intensity projection of hepatocyte spheroid co-cultured with microvessels for 7 days and stained against albumin (green) and CD31 (red). Scale bar: 200  $\mu\text{m}$ . **b** Maximum intensity projection of hepatocyte organoids co-cultured with microvessels for 21 days and stained against albumin (green) and CD31 (red). Scale bar: 200  $\mu\text{m}$ . **c** Single-plane confocal images of hepatocyte spheroid co-cultured with microvessels for 7 days and stained against albumin (green) and CD31 (red). Lumenized spaces are observable in the vessels connecting the main tubes to the hepatocyte spheroid (I, white arrow) and in close proximity of hepatocytes (ii, white arrow). Scale bar: 200  $\mu\text{m}$  (i) and 50  $\mu\text{m}$  (ii). **d** Cryo-sections of spheroids co-cultured for 1 (i), 4 (ii), and 7 (iii) days on microvascular beds stained against albumin (green), CD31 (red), and nuclei (blue). White arrow indicates penetration of CD31+endothelial cells inside the hepatocyte spheroid. Scale bar: 200  $\mu\text{m}$ . **e** EM images of sections of hepatocyte organoids co-cultured with microvessels for 7 days indicating endothelial cells (EC) with distinct lumen (i) and vascular-hepatic contact point (ii) with intracellular pinocytic vesicles (iii, white arrow). Scale bar: 10  $\mu\text{m}$ . **f** Schematic depiction of flow through the chip to assess perfusability of vascularized liver cultures using 150-KDa FITC-labeled dextran. **g** Over-time fluorescence microscopy images of 150-KDa FITC-labeled dextran perfusing a hepatocyte spheroid co-cultured for 7 days with microvessels. Dotted ellipse indicates FITC-labeled dextran emerging from the spheroid and flowing in the lateral perfusion channel

as sinusoidal obstruction syndrome (SOS). Its proposed mechanism of toxicity involves glutathione depletion in liver endothelial cells [37], followed by apoptosis of these cells and their extrusion into sinusoids, leading to obstruction and congestion and subsequent reduction of blood flow [48]. Therefore, it was investigated whether a vascularized liver spheroid model could capture congestion and loss of perfusability upon administration of Azathioprine (Fig. 4a). We first assessed whether AZA appears to be toxic to the culture as a whole. For this, we exposed vascularized and non-vascularized hepatocyte spheroids to a dose range of AZA and we assessed viability using a commercially available intracellular ATP readout. We measured ATP release in the graft chamber or in the perfusion lanes (Supplementary Fig. 8a). This allowed us to partially discriminate the toxic effect on the hepatocytes and lateral endothelial cells. Based on this initial result, we selected a concentration of 50  $\mu\text{M}$  and an exposure time of 48 h which we did not expect to result in a substantial loss of viability of the culture. Next, we tested two types of spheroids: spheroids comprising hepatocytes only (mono-spheroids) and pre-vascularized spheroids (pv-spheroids) comprising hepatocytes and RFP-HUVECs in a 20:1 ratio. We observed the formation of an intricate endothelial network inside the pv-spheroids after 2 days of aggregation (Supplementary Fig. 9a). Mono-spheroids and pv-spheroids were cultured with microvessels for 5 days, where we observed a larger extent of endothelial structures within the pv-spheroids (Supplementary Fig. 9b). Afterward, the cultures were exposed to 50  $\mu\text{M}$  AZA for 48 h. To assess the effect of AZA on the culture as a whole,

we opted for administering the drug to both, perfusion channels and graft chambers. To assess toxicity, we measured lactate dehydrogenase (LDH) released in medium samples from both the graft chamber and the perfusion channels. No significant increase in secreted LDH was observed in the perfusion channels (Fig. 4b, Supplementary Fig. 8b), indicating that the lateral vessels could tolerate exposure to AZA. LDH release in the graft chamber showed a significant increase, but only for pv-spheroids (Fig. 4c). AZA exposure did not result in evident morphological changes of the microvessels and spheroids for either mono-spheroids or pv-spheroids (Supplementary Fig. 9c). Next, cultures were stained with Sytox Green to visualize dead cells. A substantial number of dead cells was observed in the graft chamber due to AZA exposure, particularly at the regions of hepatic-endothelial interactions (Fig. 4d, e). Higher magnification confocal imaging revealed the presence of dead cells in the afferent vessels and the microvasculature in proximity to the hepatocyte spheroids (Fig. 4f). To assess whether congestion of microvasculature with dead cells caused impaired perfusion as observed during VOD, perfusability of the two types of spheroid cultures was assessed. FITC-labeled dextran was added to one lateral vessel, and perfusion toward the second lateral vessel was observed (Fig. 4g). Mono-spheroid and pv-spheroid cultures were perfusable in 25.4% and 57.5% of the cases, respectively, whereas none of the AZA-exposed cultures was perfusable (Fig. 4h). Taken together, these results demonstrate that congestion of microvasculature due to AZA exposure could be recapitulated in a vascularized liver model and that FITC-dextran perfusability could be utilized as a functional readout.

## Discussion

In vitro grafting of tissues is at the pinnacle of cell culture, adding an element that otherwise could only be achieved in vivo, i.e., through xenografting techniques. Microfluidic cell culture techniques are ideally suited for providing the perfusable microvascular network, and the open-top channel approach makes these amenable to receiving a donor tissue, the dimensions of which may well exceed those of the microfluidic channel. In this study, we demonstrated clear feasibility of in vitro grafting by example of vascularization of liver tissue. We demonstrated that the liver construct could be fluidically connected to the microfluidic vascular bed and subsequently perfused. Moreover, we showed conceptual application of the vascularized system by mimicking veno-occlusive disease and providing loss of perfusability as a phenotypic readout. We propose, therefore, a viable, robust, easy-to-use, and versatile platform to develop vascularized in vitro cultures. In this study, we focused on liver as a testbed for demonstrating the handling and capabilities

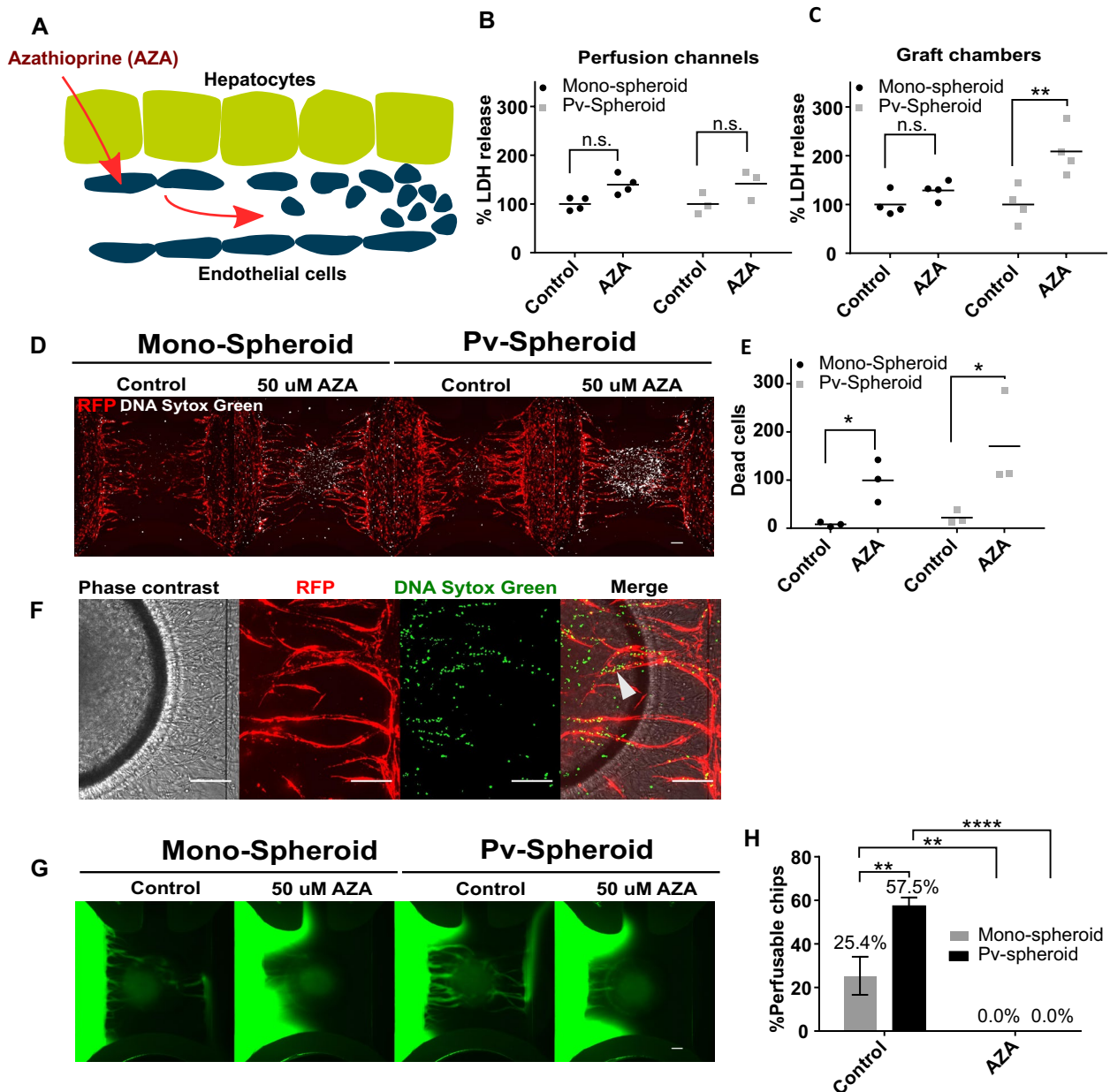


**Fig. 4** Vascularized human liver model of toxin-induced veno-occlusive disease. **a** A schematic diagram of Azathioprine-induced hepatic veno-occlusive disease. **b** Perfusion lane LDH release upon exposure to 50  $\mu$ M azathioprine (AZA) for 48 h (days 5–7 of co-culture with microvessels). Dots represent individual chips, line represents mean,  $n=3-4$ , significance was calculated using two-way ANOVA and shown as non-significant (n.s., Tukey's multiple comparison test,  $P>0.05$ ). **c** Graft chamber LDH release upon exposure of 50  $\mu$ M azathioprine for 48 h (days 5–7 of co-culture with microvessels). Dots represent individual chips, line represents mean,  $n=3-4$ . Significance was calculated using two-way ANOVA (Tukey's multiple comparison test, n.s.,  $P>0.05$ ,  $**P<0.01$ ) **d** Fluorescent images overlay of RFP-HUVEC (red) with dead cells (white) after 48 h exposure to 50  $\mu$ M AZA. **e** Quantification of dead cells in the graft chamber upon expo-

sure to 50  $\mu$ M AZA. Dots represent individual chips, line represents mean,  $n=3$ , significance was calculated using two-way ANOVA (Tukey's multiple comparison test,  $*P<0.05$ ). **f** representative images of pre-vascularized spheroid cultures exposed to 50  $\mu$ M AZA indicating the presence of dead cells inside intact vessels (white arrow). Scale bar=200  $\mu$ m. **g** Representative fluorescent images of FITC-labeled dextran after 5 min of perfusion. Dotted ellipse indicates FITC-labeled dextran emerging from the spheroid and flowing in the lateral perfusion channel. **h** Percentage of perfusable chips/Organo-Plate (8 chips/condition in a total of five plates) after AZA treatment. Bar represents mean  $\pm$  SEM,  $n=5$ . Significance was calculated using two-way ANOVA (Tukey's multiple comparison test,  $*P<0.05$ ,  $****P<0.0001$ )

of the platform. While more investigation is needed to fully capture the effect of vascularization on hepatic function, we were able to assess and confirm a functional hepatic population in a vascularized context. We further envision flow-cytometry as a future direction for further hepatic characterization.

In this study, we used three types of liver tissue constructs: liver spheroids, pre-vascularized liver spheroids, and liver organoids. Vascular beds in the presence of both liver spheroids and pre-vascularized spheroids underwent clear anastomosis. However, engraftment of pre-vascularized hepatic spheroids yielded a twofold higher success rate of forming a culture that could be perfused completely. We can, thus, conclude that constructs with endogenous endothelium are more likely to produce a functional network, a strategy that has also proven successful *in vivo* [49, 50]. Liver organoids did not convincingly induce anastomosis or subsequent perfusability. We suspect that the composition of the growth factor-rich medium used for organoids is the primary cause for this as many Hep-medium components (HGF, EGF, FGF7, and FGF10) are known to support or induce angiogenesis [51–54]. Indeed, HGF alone was capable of preventing regression of microvasculature in the absence of hepatic organoids. Additionally, we suspect that the existence of a collagen–Matrigel interface might hinder further vasculature elongation, thus, preventing complete interconnection. Further study would include reduction in growth factors in the Hep-medium to promote local gradients, as well as investigating alternatives to Matrigel which might pose a significant hindrance for vascular development.

We mimicked induction of VOD by exposure to azathioprine. While having a marginal toxic effect on the culture as a whole, azathioprine had a profound effect on the perfusability of the network. In addition, higher magnification confocal imaging revealed the presence of dead cells in the afferent vessels and the microvasculature in proximity to the hepatic spheroids. Interestingly, while LDH was not substantially increased in mono-spheroids, we did observe graft chamber elevation after treatment for cultures with pre-vascularized spheroids. This suggests that cell death did occur but predominantly in locations with dense microvascular structures.

For this study, we used HUVECs to form the vascular bed, study interaction with the target tissue, and model disease. HUVECs are a convenient source of endothelial cells that are widely available, form robust tubes, and undergo reproducible angiogenesis in our platform. Future work will focus on incorporating Liver sinusoidal endothelium (LSECs) which is a highly specialized form of endothelium that is, among other things, characterized by fenestrae. These small openings act as a selective “sieve” and allow for bidirectional exchange of molecules between sinusoidal blood and liver parenchyma [55]. Inclusion of LSECs could be

done by either growing them as a vascular bed or incorporating them with the liver spheroid and connecting them to the host vascular bed. In addition, we foresee the incorporation of other non-parenchymal cells, including stellate and Kupffer cells. We expect that such co-cultures aid long-term stability and metabolic competence of the *in vitro* culture and allow studying disease conditions such as liver fibrosis, steatosis, and possibly even using the model to assess liver infection by, for example, Hepatitis B-Virus and malaria-causing parasites.

We investigated the grafting of spheroids composed of cells from an immortalized cell line and organoids derived from liver stem cells. Another source of liver material would be tissue slices from donor livers. In that case, the tissue includes endogenous endothelium that could be used to study its ability to connect to the host vascular bed when in a sufficiently viable state. Another route to study liver vascularization is to use stem cell-derived organoids that undergo the various stages of embryonic development [56]. Such organoids are typically known to comprise all parenchymal and non-parenchymal cells present in the liver. In this case, it would be highly interesting to study the connection of endogenous endothelium with the host vascular bed. We anticipate that the timing of the grafting step and tuning of growth factors will prove crucial for effective co-development of the liver organoid and its vascular structure.

Although we focused on the liver as a proof-of-concept organ in this publication, the platform is, in essence, applicable to the vascularization of any tissue. We anticipate that such added vasculature will become crucial in the rapidly developing organoid field, potentially leading to, e.g., blood–brain barrier type endothelium in brain organoids [57], perfused glomeruli in kidney organoids [58, 59], and functional beta islets for pancreatic organoids [60].

The platform also holds promise to vascularize tumor tissue. Today tumor vascularization is typically studied in patient-derived xenografts (PDX), where tumor explants are implanted in immunodeficient or humanized mice. These models are typically exposed to therapeutic compounds to study their efficacy on a personalized level. PDX models are valuable due to their intrinsically complex microenvironment. However, their establishment is very time consuming, cumbersome, and with variable success rates. Therefore, such PDX studies are primarily used for retrospective rather than prospective studies [61, 62]. An *in vitro* grafting protocol holds the promise of being faster, more reproducible, more cost effective as well as easier to analyze than classical PDX approaches. Alternatively, this platform could be used to generate more relevant PDX explant cultures currently used in drug and biomarker discovery. Grafted PDX explant cultures would eventually allow for the inclusion of relevant immune cells, overcoming in part a limitation of using PDX models in immune oncology [63–65].

Until today, the study of tissue vascularization is limited to laboratories that have access to animal testing facilities. The platform demonstrated here shows clear proof-of-concept of vascularization of tissues *in vitro*. Not only was the concept of vascularizing *in vitro* proven feasible, but the platform also allows routine experimentation with sufficient throughput, fully compatible with (automated) microscopes and robotic handling. The accessibility of the platform for any laboratory around the world and its usability by any cell culture biologist will provide a great push forward toward routine inclusion of perfused vasculature in tissue culture protocols.

**Supplementary Information** The online version contains supplementary material available at <https://doi.org/10.1007/s10456-022-09842-9>.

**Acknowledgements** We would like to thank Rumaisha Annida and members of the Microscopy CORE Lab of M4I-FHML of Maastricht University for their technical support and Kristin Bircsak for valuable comments. We also would like to thank Mimetas Biocore team including Kristina Bishard, Arthur Stok, Manon Haarmans, and Julia Grasegger. This project has received funding from the European Union's Horizon 2020 research and innovation program under grant agreement No 848429 and Interreg, project Biomat on microfluidic chip 433. AN and FB have received funding from the European Union's Horizon 2020 research and innovation program under the Marie Skłodowska-Curie grant agreement No 641639 and No 812616, respectively. This project was partly funded by an innovation loan (IK17088) from the Dutch Ministry of Economic Affairs and Climate. This work was supported by partners of Regenerative Medicine Crossing Borders ([www.regmedxb.com](http://www.regmedxb.com)), powered by Health-Holland, Top Sector Life Sciences & Health.

**Author contributions** PV, DK and SJT: *Conceptualization*. FB, SP, SR, BK, AN, SBG, KQ, MM, MCC, RD, and DK: *Methodology*. TO, AN, and EW: *Software*. PV, SJT, AN, and KD: *Microfluidics*. TO, EW, and SP: *Automation*. DH, DD, HH and HC: *Hepatic organoids*. CL-I and PJP: *TEM*. FB and SP: *Formal analysis*. DK, HLL, and BR: *Project administration*. PV, JJ, HLL, and HC: *Resources*. FB, SP, and FS: *Data curation and schematics*. FB, SP, PV, and DK: *Writing*.

**Data availability** All the data supporting the findings of this study are available from the corresponding author on reasonable request.

## Declarations

**Competing interest** Paul Vulto, Dorota Kurek, Flavio Bonanini, Sara Previdi, Sander de Ruiter, Bart Kramer, Rumaisha Annida, Silvia Bonilla García, Karla Queiroz, Marine Meyer, Maria Clapés Cabrer, Roelof Dinkelberg, Thomas Olivier, Arnaud Nicolas, Karel Domansky, Erik Walinga, Jos Joore, Henriette L. Lanz, Sebastiaan J. Trietsch, and Bob Rondan are employees of Mimetas BV, which is marketing the OrganoPlate Graft and Paul Vulto, Jos Joore, and Sebastiaan J. Trietsch are shareholders of Mimetas BV. OrganoPlate is a registered trademark of Mimetas BV. Hans Clevers is inventor on several patents related to organoid technology; his full disclosure is given at <https://www.uu.nl/staff/JCClevers/>. Since March 2022, HC is Head of Pharma Research and Early Development (pRED) of F. Hoffmann-La Roche Ltd, Basel, Switzerland. The authors have no additional financial interests.

**Open Access** This article is licensed under a Creative Commons Attribution 4.0 International License, which permits use, sharing, adaptation, distribution and reproduction in any medium or format, as long as you give appropriate credit to the original author(s) and the source, provide a link to the Creative Commons licence, and indicate if changes were made. The images or other third party material in this article are included in the article's Creative Commons licence, unless indicated otherwise in a credit line to the material. If material is not included in the article's Creative Commons licence and your intended use is not permitted by statutory regulation or exceeds the permitted use, you will need to obtain permission directly from the copyright holder. To view a copy of this licence, visit <http://creativecommons.org/licenses/by/4.0/>.

## References

- Fennema E, Rivron N, Rouwkema J, van Blitterswijk C, De Boer J (2013) Spheroid culture as a tool for creating 3D complex tissues. *Trends Biotechnol* 31(2):108–115
- Prior N, Inacio P, Huch M (2019) Liver organoids: from basic research to therapeutic applications. *Gut* 68(12):2228–2237
- Grebenyuk S, Ranga A (2019) Engineering organoid vascularization. *Front Bioeng Biotechnol* 7(March):1–12
- Si-Tayeb K, Lemaigre FP, Duncan SA (2010) Organogenesis and development of the liver. *Dev Cell* 18(2):175–189
- Ni Y, Li JM, Liu MK, Zhang TT, Wang DP, Zhou WH et al (2021) Pathological process of liver sinusoidal endothelial cells in liver diseases. *World J Gastroenterol* 23(43):7666–7677
- Glicklis R, Merchuk JC, Cohen S (2004) Modeling mass transfer in hepatocyte spheroids via cell viability, spheroid size, and hepatocellular functions. *Biotechnol Bioeng* 86(6):672–680
- Edmondson R, Broglie JJ, Adcock AF, Yang L (2014) Three-dimensional cell culture systems and their applications in drug discovery and cell-based biosensors. *Assay Drug Dev Technol* 12(4):207–218
- Matsumoto K, Yoshitomi H, Rossant J, Zaret KS (2001) Liver organogenesis promoted by endothelial cells prior to vascular function. *Science* 294(5542):559–563
- Han S, Tan C, Ding J, Wang J, Ma'ayan A, Gouon-Evans V (2018) Endothelial cells instruct liver specification of embryonic stem cell-derived endoderm through endothelial VEGFR2 signaling and endoderm epigenetic modifications. *Stem Cell Res* 30:163–170
- Han S, Dziedzic N, Gadue P, Keller GM, Gouon-Evans V (2011) An endothelial cell niche induces hepatic specification through dual repression of Wnt and notch signaling. *Stem Cells* 29(2):217–228
- Poisson J, Lemoine S, Boulanger C, Durand F, Moreau R, Valla D et al (2017) Liver sinusoidal endothelial cells: physiology and role in liver diseases. *J Hepatol* 66(1):212–227
- Ware BR, Durham MJ, Monckton CP, Khetani SR (2018) A cell culture platform to maintain long-term phenotype of primary human hepatocytes and endothelial cells. *Cmgh* 5(3):187–207
- Timmins N, Dietmair S, Nielsen L (2004) Hanging-drop multicellular spheroids as a model of tumour angiogenesis. *Angiogenesis* 7(2):97–103
- Inamori M, Mizumoto H, Kajiwaru T (2009) An approach for formation of vascularized liver tissue by endothelial cell-covered hepatocyte spheroid integration. *Tissue Eng Part A* 15(8):2029–2037
- Sasaki K, Akagi T, Asaoka T, Eguchi H, Fukuda Y, Iwagami Y et al (2017) Construction of three-dimensional vascularized functional human liver tissue using a layer-by-layer cell coating technique. *Biomaterials* 133:263–274

16. Jin Y, Kim J, Lee JS, Min S, Kim S, Ahn DH et al (2018) Vascularized liver organoids generated using induced hepatic tissue and dynamic liver-specific microenvironment as a drug testing platform. *Adv Func Mater* 28(37):1–15
17. Takebe T, Sekine K, Enomura M, Koike H, Kimura M, Ogaeri T et al (2013) Vascularized and functional human liver from an iPSC-derived organ bud transplant. *Nature* 499(7459):481–484
18. Irudayaswamy A, Muthiah M, Zhou L, Hung H, Jumat NHB, Haque J et al (2018) Long-term fate of human fetal liver progenitor cells transplanted in injured mouse livers. *Stem Cells* 36(1):103–113
19. Li J, Xing F, Chen F, He L, So KF, Liu Y et al (2019) Functional 3D human liver bud assembled from MSC-derived multiple liver cell lineages. *Cell Transplant* 28(5):510–521
20. Singh VP, Pratap K, Sinha J, Desiraju K, Bahal D, Kukreti R (2016) Critical evaluation of challenges and future use of animals in experimentation for biomedical research. *Int J Immunopathol Pharmacol* 29(4):551–561
21. van Duinen V, Trietsch SJ, Joore J, Vulto P, Hankemeier T (2015) Microfluidic 3D cell culture: from tools to tissue models. *Curr Opin Biotechnol* 35:118–126
22. Du Y, Li N, Yang H, Luo C, Gong Y, Tong C et al (2017) Mimicking liver sinusoidal structures and functions using a 3D-configured microfluidic chip. *Lab Chip* 17(5):782–794
23. Li X et al (2017) A glass-based, continuously zoned and vascularized human liver acinus microphysiological system (vLAMPS) designed for experimental modeling of diseases and ADME/TOX. *Physiol Behav* 176(10):139–48
24. Jang KJ, Otieno MA, Ronxhi J, Lim HK, Ewart L, Kodella KR et al (2019) Reproducing human and cross-species drug toxicities using a Liver-Chip. *Sci Transl Med*. <https://doi.org/10.1126/scitranslmed.aax5516>
25. Paek J, Park SE, Lu Q, Park KT, Cho M, Oh JM et al (2019) Microphysiological engineering of self-assembled and perfusable microvascular beds for the production of vascularized three-dimensional human microtissues. *ACS Nano* 13(7):7627–7643
26. Sobrino A, Phan DTT, Datta R, Wang X, Hachey SJ, Romero-López M et al (2016) 3D microtumors in vitro supported by perfused vascular networks. *Sci Rep* 6(May):1–11
27. Phan DTT, Wang X, Craver BM, Sobrino A, Zhao D, Chen JC et al (2017) A vascularized and perfused organ-on-a-chip platform for large-scale drug screening applications. *Lab Chip* 17(3):511–520
28. Zhang S, Wan Z, Kamm RD (2021) Vascularized organoids on a chip: strategies for engineering organoids with functional vasculature. *Lab Chip* 21(3):473–488
29. Oh S, Ryu H, Tahk D, Ko J, Chung Y, Lee HK et al (2017) “Open-Top” microfluidic device for in vitro three-dimensional capillary beds. *Lab Chip* 17(20):3405–3414
30. Nashimoto Y, Hayashi T, Kunita I, Nakamasu A, Torisawa YS, Nakayama M et al (2017) Integrating perfusable vascular networks with a three-dimensional tissue in a microfluidic device. *Integr Biol (United Kingdom)* 9(6):506–518
31. Nashimoto Y, Okada R, Hanada S, Arima Y, Nishiyama K, Miura T et al (2019) Vascularized cancer on a chip: the effect of perfusion on growth and drug delivery of tumor spheroid. *Biomaterials* 2020(229):119547
32. Lin DSY, Rajasekar S, Marway MK, Zhang B (2020) From model system to therapy: scalable production of perfusable vascularized liver spheroids in “open-Top” 384-well plate. *ACS Biomater Sci Eng* 7:2964–2972
33. De Fontbrune FS, Mal H, Dauriat G, Brugière O, Biondi G, Taillé C et al (2007) Venous-occlusive disease of the liver after lung transplantation. *Am J Transplant* 7(9):2208–2211
34. Jacobi AM, Feist E, Rudolph B, Burmester GR (2004) Sinusoidal dilatation: a rare side effect of azathioprine. *Ann Rheum Dis* 63(12):1702–1703
35. Liano F, Moreno A, Matesanz R, Teruel JL, Redondo C, Garcia-Martin F et al (1989) Venous-occlusive hepatic disease of the liver in renal transplantation: Is azathioprine the cause? *Nephron* 51(4):509–516
36. Katzka DA, Saul SH, Jorkasky D, Sigal H, Reynolds JC, Soloway RD (1986) Azathioprine and hepatic venoocclusive disease in renal transplant patients. *Gastroenterology* 90(2):446–454
37. Deleve LD, Wang X, Kuhlenkamp JF, Kaplowitz N (1996) Toxicity of azathioprine and monocrotaline in murine sinusoidal endothelial cells and hepatocytes: the role of glutathione and relevance to hepatic venoocclusive disease. *Hepatology* 23(3):589–599
38. Guzm C, Castell V, Donato MT, Martorell A, Torre NA, De D (2016) Human upcyte hepatocytes: characterization of the hepatic phenotype and evaluation for acute and long-term hepatotoxicity routine testing. *Toxicol Sci* 152(1):214–229
39. Hu H, Gehart H, Artegiani B, Peters PJ, De JYP, Clevers H et al (2018) Long-term expansion of functional mouse and human hepatocytes as 3D organoids. *Cell* 175:1591–1606
40. Yildirim E, Trietsch SJ, Joore J, van den Berg A, Hankemeier T, Vulto P (2014) Phaseguides as tunable passive microvalves for liquid routing in complex microfluidic networks. *Lab Chip* 14(17):3334–3340
41. Vulto P, Podszun S, Meyer P, Hermann C, Manz A, Urban GA (2011) Phaseguides: a paradigm shift in microfluidic priming and emptying. *Lab Chip* 11(9):1596–1602
42. Trietsch SJ, Naumovska E, Kurek D, Setyawati MC, Vormann MK, Wilschut KJ et al (2017) Membrane-free culture and real-time barrier integrity assessment of perfused intestinal epithelium tubes. *Nat Commun*. <https://doi.org/10.1038/s41467-017-00259-3>
43. Jang M, Neuzil P, Volk T, Manz A, Kleber A (2015) On-chip three-dimensional cell culture in phaseguides improves hepatocyte functions in vitro. *Biomicrofluidics* 9(3):34113. <https://pubmed.ncbi.nlm.nih.gov/26180570>
44. Jung O, Tung Y-T, Sim E, Chen Y-C, Lee E, Ferrer M et al (2022) Development of human-derived, three-dimensional respiratory epithelial tissue constructs with perfusable microvasculature on a high-throughput microfluidics screening platform. *Biofabrication* 1(14):25012
45. Wevers NR, van Vught R, Wilschut KJ, Nicolas A, Chiang C, Lanz HL et al (2016) High-throughput compound evaluation on 3D networks of neurons and glia in a microfluidic platform. *Sci Rep* 6(1):38856. <https://doi.org/10.1038/srep38856>
46. Van Duinen V, Ramakers DZC, Vulto AJVZP (2019) Perfused 3D angiogenic sprouting in a high-throughput in vitro platform. *Angiogenesis* 22(1):157–165
47. Hu H, Gehart H, Artegiani B, López-Iglesias C, Dekkers F, Basak O et al (2018) Long-term expansion of functional mouse and human hepatocytes as 3D organoids. *Cell* 175(6):1591–1606
48. Kumar S, DeLeve LD, Kamath PS, Tefferi A (2003) Hepatic veno-occlusive disease (sinusoidal obstruction syndrome) after hematopoietic stem cell transplantation. *Mayo Clin Proc* 78(5):589–598
49. Shahar B-S, Shira L, Uri M, Shulamit L (2019) Mature vessel networks in engineered tissue promote graft–host anastomosis and prevent graft thrombosis. *Proc Natl Acad Sci* 116(8):2955–2960. <https://doi.org/10.1073/pnas.1814238116>
50. Mishra R, Roux BM, Posukonis M, Bodamer E, Brey EM, Fisher JP, et al (2016) Effect of prevascularization on in vivo vascularization of poly(propylene fumarate)/fibrin scaffolds. *Biomaterials* 77:255–66. <https://pubmed.ncbi.nlm.nih.gov/26606451>. Accessed 22 Oct, 2015

51. Gillis P, Savla U, Volpert OV, Jimenez B, Waters CM, Panos RJ et al (1999) Keratinocyte growth factor induces angiogenesis and protects endothelial barrier function. *J cell Sci* 112(1):2049–2057
52. McVicar CM, Rice-McCaldin A, Curtis T, Stitt AW, Gardiner TA (2007) Angiogenesis induced by EGF is mediated by autocrine VEGF. *Invest Ophthalmol Vis Sci* 48(13):1379
53. Liu F, Li G, Deng L, Kuang B, Li X (2017) The roles of FGF10 in vasculogenesis and angiogenesis. *Biomed Res* 28:1329–1332
54. Xin X, Yang S, Ingle G, Zlot C, Rangell L, Kowalski J et al (2001) Hepatocyte growth factor enhances vascular endothelial growth factor-induced angiogenesis in vitro and in vivo. *Am J Pathol* 158(3):1111–1120
55. Braet F, Wisse E (2002) Structural and functional aspects of liver sinusoidal endothelial cell fenestrae: a review. *Comp Hepatol* 1:1–17
56. Ouchi R, Togo S, Kimura M, Shinozawa T, Koido M, Koike H et al (2019) Modeling steatohepatitis in humans with pluripotent stem cell-derived organoids. *Cell Metab* 30(2):374–384
57. Cakir B, Xiang Y, Tanaka Y, Kural MH, Parent M, Kang YJ et al (2019) Engineering of human brain organoids with a functional vascular-like system. *Nat Methods* 16(11):1169–1175
58. Homan KA, Gupta N, Kroll KT, Kolesky DB, Skylar-Scott M, Miyoshi T et al (2019) Flow-enhanced vascularization and maturation of kidney organoids in vitro. *Nat Methods* 16(3):255–262
59. Koning M, van den Berg CW, Rabelink TJ (2020) Stem cell-derived kidney organoids: engineering the vasculature. *Cell Mol Life Sci* 77:2257–2273
60. Takahashi Y, Takebe T, Taniguchi H (2018) Methods for generating vascularized islet-like organoids via self-condensation. *Curr Protoc Stem Cell Biol* 45(1):1–12
61. Koga Y, Ochiai A (2019) Systematic review of patient-derived xenograft models for preclinical studies of anti-cancer drugs in solid tumors. *Cells* 8(5):418
62. Lanz HL, Saleh A, Kramer B, Cairns J, Ng CP, Yu J et al (2017) Therapy response testing of breast cancer in a 3D high-throughput perfused microfluidic platform. *BMC Cancer* 17(1):1–11
63. Powley IR, Patel M, Miles G, Pringle H, Howells L, Thomas A et al (2020) Patient-derived explants (PDEs) as a powerful pre-clinical platform for anti-cancer drug and biomarker discovery. *Br J Cancer* 122(6):735–744
64. Meijer TG, Jager A, Gent DC (2017) Ex vivo tumor culture systems for functional drug testing and therapy response prediction. *Future Sci OA* 3(2):FSO190
65. Ghosh S, Prasad M, Kundu K, Cohen L, Yegodayev KM, Zorea J et al (2019) Tumor tissue explant culture of patient-derived xenograft as potential prioritization tool for targeted therapy. *Front Oncol* 9(1):1–12

**Publisher's Note** Springer Nature remains neutral with regard to jurisdictional claims in published maps and institutional affiliations.